Identification of *in vitro* and *in vivo* oncolytic effect in colorectal cancer cells by Orf virus strain NA1/11

DAXIANG CHEN[1,2*], RUIXUE WANG[3*], MINGJIAN LONG[1,4*], WEI LI[1], BIN XIAO[5], HAO DENG[1], KONGYAN WENG[1], DAOYUAN GONG[3], FANG LIU[3], SHUHONG LUO[1,3] and WENBO HAO[1]

[1]Key Laboratory of Antibody Engineering of Guangdong Higher Education Institutes,
School of Laboratory Medicine and Biotechnology, Southern Medical University, Guangzhou, Guangdong 510515;
[2]Department of Laboratory Medicine, Dermatology Hospital, Southern Medical University, Guangzhou, Guangdong 510091;
[3]Department of Laboratory Medicine, School of Stomatology and Medicine, Foshan University, Foshan, Guangdong 528000;
[4]Department of Laboratory Medicine, The Fifth Affiliated Hospital of Southern Medical University,
Guangzhou, Guangdong 510900; [5]Department of Laboratory Medicine,
General Hospital of Southern Theatre Command of PLA, Guangzhou, Guangdong 510010, P.R. China

Abstract. Orf virus (ORFV) is a favorable oncolytic viral carrier in research, and ORFV strain NZ2 has been revealed to have antitumor effects in animal models mediated by immunoregulation profile. However, the antitumor effects triggered by the ORFV in colorectal cancer (CRC) cells is poorly characterized. The *in vivo* and *in vitro* roles of ORFV in CRC were determined using western blotting, colony formation, CCK-8, wound scratch assay, qPCR, and animal models. Furthermore, cytokine antibody chip assay, flow cytometry, western blotting, and immunohistochemical (IHC) assays were conducted to explore the potential mechanism of ORFV. The present data revealed that ORFV strain NA1/11 infected and inhibited the *in vitro* growth and migration of CRC cells. By establishing a CRC model in Balb/c mice, it was revealed that ORFV strain NA1/11 significantly inhibited the *in vivo* growth and migration of CRC cells. A cytokine antibody array was utilized to obtain a more comprehensive profile revealing the differentially expressed cytokines in ORFV infection. Cytokines, such as IL-7, IL-13, IL-15, CD27, CD30, pentraxin 3, and B lymphocyte chemoattractant (BLC), were upregulated. Axl, CXCL16, ANG-3, MMP10, IFN-γ R1 and VEGF-B were downregulated. The results indicated that ORFV played roles in the regulation of key factors relevant to apoptosis, autoimmunity/inflammation, angiogenesis, and the cell cycle. Finally, data was presented to validate that ORFV infection induces oncolytic activity by enhancing apoptosis *in vivo* and *in vitro*. In conclusion, ORFV could be an oncolytic virus for CRC therapy.

Correspondence to: Dr Shuhong Luo, Department of Laboratory Medicine, School of Stomatology and Medicine, Foshan University, 5 Hebin Road, Chancheng, Foshan, Guangdong 528000, P.R. China
E-mail: sluo815@gmail.com

Dr Wenbo Hao, Key Laboratory of Antibody Engineering of Guangdong Higher Education Institutes, School of Laboratory Medicine and Biotechnology, Southern Medical University, 1838 Guangzhou Avenue North, Baiyun, Guangzhou, Guangdong 510515, P.R. China
E-mail: haowa@126.com

*Contributed equally

Abbreviations: CRC, colorectal cancer; ORFV, Orf virus; NK, natural killer; DC, dendritic cells; IL-1RA, IL-1 receptor antagonist; MOI, multiplicities of infection; OD, optical density; RAGE, receptor of advanced glycosylation end product; MMP10, matrix metallopeptidase 10; ECL, enhanced chemiluminescence; PVDF, polyvinylidene difluoride; FBS, fetal bovine serum; OFTu, ovine fetal turbinate; VEGF, vascular endothelial growth factor; DLL4, delta-like canonical Notch ligand 4; BLC, B lymphocyte chemoattractant

Key words: Orf virus, antitumor, colorectal cancer, cytokines, apoptosis

Introduction

Oncolytic viruses, characterized by their preferential infection, replication and destruction of tumor cells and cancer-associated endothelial cells, have become a major topic for basic research and consequent clinical applications in novel tumor therapy strategies (1). Concomitant antitumor immune responses often exist as well (2). In recent decades, oncolytic viral therapy has aroused widespread interest and great progress has been achieved (3). Various oncolytic viruses have been studied and some have already been developed for treatments agents, such as adenovirus, herpes simplex virus type I, and the vaccinia virus (4,5). Imlygic (talimogene laherparepvec; T-VEC) is the first oncolytic virus approved for melanoma therapy by the USFDA for cases where lesions are in the skin and lymph nodes and cannot be completely removed by surgery (6). The safety and effectiveness of oncolytic viruses have been widely accepted (6).

Orf virus (ORFV) is a prototype member of the genus *Parapoxvirus*, belonging to *Poxviridae*, which can cause contagious pustular stomatitis, an acute mucocutaneous infection in sheep and goats, and is usually self-limiting (7,8). With an increasing number of comprehensive studies on its molecular, biological and immunological characteristics, especially given its vigorous and particular immunomodulatory properties, ORFV has been proposed as a potential oncolytic virus vector (8-10).

ORFV is known to have a strong immunomodulating activity against the host. ORFV can rapidly mediate innate and adaptive immune responses in the body. Upon infection by ORFV, neutrophils, natural killer (NK) cells and dendritic cells (DC) are enriched at the infection sites, various types of cells in the innate immune system are activated, and several key cytokines are secreted (8). Notably, ORFV induces mainly the Th1 immune response in the early stages of infection where the classical cytokines IFN-γ, TNF, IL-6, IL-8, IL-12 and IL-18 are secreted from the peripheral immune cells (8,11). Then, the Th2 type immune response appears with the secretion of IL-4, IL-1 receptor antagonist (IL-1RA), and IL-10 (12).

A live or inactivated ORFV can induce a strong antitumor immune response in murine models of multiple tumors. Fiebig *et al* (9) were the first to report that inactivated ORFV mediates antitumor effects in various tumor models, including the murine syngeneic B16F10 melanoma and MDA-MB-231 human breast cancer xenograft, and revealed that NK cells play an important role in the antitumor effects of ORFV. Anti-mouse NK-1.1 antibody partially inhibited its antitumor activity by inhibiting the activity of NK and NKT cells. Moreover, when IFN-γ was neutralized, the inhibitory effects of ORFV disappeared (9). Inactivated ORFV inhibited tumor growth of MDA-MB-231 tumor-bearing NOD/LtSz-scid/j mice which lacked NK and functional T- and B-lymphocytes (9). Rintoul *et al* (11) confirmed that live ORFV possessed antitumor effects through activation of NK cells and by inducing secretion of cytokines IFN-γ and granzyme B. A previous study has found that surgery mediates the disfunction of NK cells, but ORFV injection during surgery can improve the function of NK cells, thereby reducing intra-operative metastasis and prolonging the survival time (13). A better understanding of the molecular mechanisms underlying the antitumor effects of ORFV will be beneficial to further develop ORFV as oncolytic vectors for human tumor treatment.

In prior studies, researchers have revealed some mechanisms through which oncolytic viruses exert oncolytic functions (14-16): direct tumoricidal cytotoxicity and activation of host antitumor immune responses. Referring to functional characteristics of oncolytic viruses and complicated immunoregulation function of ORFV (17-19), the present study used high-throughput screening methods to investigate the ORFV-mediated regulation of cytokine expression. In the present study, the antitumor activity of ORFV strain NA1/11 was investigated through *in vitro* cell experiments and *in vivo* animal studies.

Materials and methods

Reagents. The antibodies for cleaved caspase-3 (product no. 9664), cleaved caspase-9 (product no. 7237), Smac (product no. 15108), β-tubulin (product no. 2146), PARP (product no. 9542) were obtained from Cell Signaling Technology, Inc. Annexin V/7-AAD Apoptosis Detection Kit was obtained from Nanjing KeyGen Biotech Co., Ltd. The enhanced chemiluminescence (ECL) detection kit was acquired from Pierce; Thermo Fisher Scientific, Inc. The Cell Counting Kit-8 (CCK-8) reagent was purchased from Dojindo Molecular Technologies, Inc. Polyvinylidene difluoride (PVDF) membranes were obtained from EMD Millipore. Fetal bovine serum, MEM, DMEM, streptomycin and penicillin were from Gibco; Thermo Fisher Scientific, Inc. All other chemicals and solvents were of analytical grade.

Cell lines and virus. CRC cell lines (LoVo, HCT116, RKO, SW480, SW1116, Caco-2 and CT26) were purchased from the cell bank of the Chinese Academy of Sciences. All CRC cells were cultured in DMEM supplemented with 10% fetal bovine serum (FBS). Ovine fetal turbinate (OFTu) cells were prepared as previously described (20), and maintained in MEM supplemented with 10% FBS. Orf virus (NA1/11) was isolated in our previous study (21). NA1/11Δ132-GFP is a recombinant Orf virus with the deletion of the ORFV132 gene by homologous recombination. OFTu cells were infected with NA1/11 or NA1/11Δ132-GFP (MOI =0.1) and were harvested when approximately 80-90% of the cells exhibited cytopathogenic effects (CPE). After repeated freezing and thawing, cellular debris was removed by centrifugation at 800 x g for 5 min at 4°C, and supernatants were purified by sucrose gradient ultracentrifugation. Pellets were suspended in PBS (when used for animal research), or MEM (when used for virus proliferation in cells) aliquots were frozen at -80°C. Viral titers were obtained by the median tissue culture infective dose (TCID$_{50}$) method (22).

Preparation of NA1/11Δ132-GFP recombinant ORFV. A virus recombinant transfer vector pSPV-EGFP with a high expression of green fluorescent protein (GFP) was successfully constructed (23). With pSPV-EGFP, the plasmids ORFV132F-pSPV-EGFP-ORFV132R were constructed by molecular cloning and used to transfect OFTu cells using Lipofectamine 3000 at room temperature (Invitrogen; Thermo Fisher Scientific, Inc.), after OFTu cells were infected with NA1/11 (MOI =1) for 2 h. For each well of a 6-well plate, plasmid DNA and lipid were mixed gently in 200 µl Opti-MEM media by adding 2.5 µg plasmid DNA and 5 µl Lipofectamine Reagent and incubated for 20 min at room temperature. It was necessary to replace the medium with fresh medium 4-6 h after transfection. Screening for fluorescent viral plaques was performed under a fluorescence microscope (Nikon Eclipse E400; Nikon Corporation) at a magnification of x100. After 15 rounds of plaque purification, NA1/11Δ132-GFP was obtained.

Wound-healing assay. Cells were seeded in 6-well plates at a density of 1x10^6 cells/well and cultured for 24 h. A wound was scratched in the cell lawn with a sterile 200-µl pipette tip and the cells were washed with serum-free DMEM three times to remove debris. The cells were exposed to ORFV at designated multiplicities of infection (MOI =0, 1, 5, 10). Images of wound healing progression were captured at 24 h post infection under

a light microscope (Nikon Eclipse E400) at a magnification of x100.

Crystal violet stain. CT26 and LoVo cells were seeded in 24-well plates at a density of $1x10^4$ cells/well and infected with ORFV at designated multiplicities of infection (MOI =0, 1, 5, 10). Living cells were stained with crystal violet solution (0.5% crystal violet) at room temperature for 0, 24, 48 and 72 h. Cells were washed with PBS three times to remove the debris and fixed with 500 μl methanol for 5 min at room temperature. After being washed with PBS three times to remove methanol, the cells were stained with crystal violet solution for 10 min at room temperature. The stain was removed and the plates were washed thrice with PBS. Images of the crystal violet stain were captured under a light microscope (Nikon Eclipse E400) at a magnification of x100.

CCK-8 assay. Cells were seeded at $1x10^3$ cells/well in a 96-well plate. Cells were exposed to designated multiplicities of infection (MOI =0, 1, 5, 10) for various time-points (0, 24, 48 and 72 h). The cell supernatant was removed, the CCK-8 solution (10% CCK-8 reagent diluted in DMEM supplemented with 10% FBS) was added and the cells were incubated for 2 h at 37°C in an atmosphere of 5% CO_2. The optical density (OD) was measured at 450 nm using an iMark microplate reader (iMark™; Bio-Rad Laboratories, Inc.).

Reverse transcription-quantitative (RT-q)PCR. Total RNA was extracted using TRIzol reagent (Invitrogen; Thermo Fisher Scientific, Inc.) and reverse-transcribed to cDNA using the High Capacity cDNA Reverse Transcription Kit (Thermo Fisher Scientific, Inc.). RT-qPCR was carried out with Fast SYBR™ Master Mix (Thermo Fisher Scientific, Inc.) on ABI StepOne Real-Time PCR platform according to the manufacturer's instructions (Thermo Fisher Scientific, Inc.). The primers used were as follows: E-cadherin forward, 5'-TACACTGCCCAGGA GCCAGA-3' and reverse, 5'-TGGCACCAGTGTCCGGATTA-3'; N-cadherin forward, 5'-ACCTGAACGACTGGGGGCCA-3' and reverse, 5'-TGCCAAAGCCTCCAGCAAGCA-3'; β-actin forward, 5'-TGAAGGTGACAGCAGTCGGTTG-3' and reverse, 5'-GGCTTTTAGGATGGCAAGGGAC-3'. The reaction protocol was 30 sec at 94°C, 43 cycles of 5 sec at 94°C and 34 sec at 60°C. Data were analyzed as Relative Quantitation (RQ) with respect to a calibrator sample using the $2^{-\Delta\Delta Cq}$ method (24). The results were presented as the mean ± SD from three experiments.

In vivo tumor model. In total, 12 healthy male Balb/c mice, aged from 6 to 8 weeks (body weight of 18±1.3 g), were purchased from the Laboratory Animal Center of the Southern Medical University. Animals were housed 6 per cage in the animal facility. The room temperature was maintained constant at 22±1°C and the humidity was controlled at 50-60% on a 12-h light/dark cycle. The animals had access to food and water *ad libitum*. In the CRC mouse model, CT26 cells ($5x10^5$ in 50 μl PBS) were subcutaneously injected into Balb/c mice. When the tumor volume reached 25-30 mm^3 [tumor volume (mm^3)=(1/6) × π × a^2 × b (a=width, b=length)], twelve mice were randomly divided into two groups and administrated with the following agents by intratumoral injection for a total of 4 injections in 12 days: i) PBS control; and ii)

ORFV ($1x10^8$ TCID$_{50}$). At the end of the experiment, animals were sacrificed by cervical dislocation. Excised tumors were measured. The organs and tumor tissues were fixed in 4% paraformaldehyde for subsequent IHC assay at room temperature for 24 h. For mouse lung metastasis models, $5x10^5$ CT26 cells were injected intravenously (i.v.) into 12 Balb/c mice. Mice were then treated i.v. with ORFV ($1x10^7$ TCID$_{50}$) in 100 μl of PBS, or control-treated (100 μl PBS), on days 1, 3 and 8. At 11 days after CT26 injection, mice were anesthetized with 60-120 μg/g Euthanyl (Sigma-Aldrich; Merck KGaA) and their blood and lungs were harvested. The serum was stored at -20°C for cytokine antibody array. The lung tissues were fixed in 4% paraformaldehyde at room temperature for 24 h for hematoxylin and eosin (H&E) staining, respectively. All animal procedures were reviewed and approved by the Institutional Animal Care and Use Committee at Foshan University (Foshan, China) (approval no. 20170311).

Immunohistochemistry. Tumor tissues and organs isolated from the mice were fixed with 4% paraformaldehyde at room temperature for 24 h, embedded in paraffin, and sliced (5-μm thick). The slides of the tumor tissues were immunohistochemically stained with cleaved caspase-3 (1:2,000 dilution in antibody diluent) according to the immunohistochemical (IHC) detection system kit manufacturer's instructions (product no. BD5001; Bioworld Technology, Inc.). Briefly, slides were heated at 55°C for 40 min and the dewaxing, rehydration, antigen retrieval and blocking were performed. The primary antibody was incubated at 4°C overnight. Immunostaining continued with HRP-conjugated secondary antibody (product no. BD5001; Bioworld Technology, Inc.) incubated at room temperature for 10 min according to the manufacturer's instructions. The DAB chomogen (product no. BD5001; Bioworld Technology, Inc.) was used for incubation at room temperature for 4 min followed by washing. The slides of the organs were stained with hematoxylin for 2 min and dehydrated with ethanol and xylenes, mounted and cover slipped. The images were obtained under a light microscope.

Flow cytometry. The flow cytometric assay was performed to detect apoptosis in tumor cells exposed to ORFV. CT26 tumor cells were seeded in a 6-well plate at a density of $1x10^6$ cells/well and exposed to ORFV (MOI =10) or PBS for 24 h. The collected cells were processed using Annexin V-APC/7-AAD Apoptosis Detection Kit according to the manufacturer's instructions. Apoptosis of the stained cells was detected using a LSRFortessa flow cytometer (BD Biosciences). BD FACSDiva software 4.1 (BD Biosciences) was used for analysis.

Western blot analysis. Cells exposed to ORFV were lysed in RIPA lysis buffer (cat. no. P0013C; Beyotime Institute of Biotechnology) containing 50 mM Tris (pH 7.4), 150 mM NaCl, 1% NP-40, 0.5% sodium deoxycholate, 0.1% SDS and protein inhibitors, such as sodium orthovanadate, sodium fluoride, EDTA and leupeptin. Levels of proteins were measured by bicinchoninic acid assay. The lysis was mixed with 1X SDS protein loading buffer and boiled for 15 min. For each individual sample, 30 μg of protein were loaded per lane on 12% SDS polyacrylamide gels. Proteins were electro-transferred to PVDF membranes at a constant 100 V for 60 min.

The PVDF membranes were blocked with 5% non-fat milk for 2 h at room temperature and incubated with primary antibody (with 1:1000 dilution, according to the manufacturer's protocol) overnight at 4˚C. The PVDF membranes were washed with TBST five times for 5 min per wash and incubated with HRP-conjugated antibodies, including goat anti-rabbit IgG H&L (HRP) (product code ab6721; 1:10,000 dilution) and goat anti-mouse IgG H&L (HRP) (product code ab6789; 1:2,000 dilution; both from Abcam) for 1 h at room temperature. The membranes were washed with TBST again and visualized with ECL chemiluminescence reagent (Tanon Science and Technology Co., Ltd.) using photographic film.

Cytokine antibody array. Mouse sera of the ORFV-treated and PBS-treated subjects were collected and measured, according to the manufacturer's instructions, with a semi-quantitative mouse cytokine antibody array (RayBio Human Cytokine Antibody Array G series 4000; RayBiotech, Inc.) which detects 200 cytokines in one experiment. Briefly, the samples were added to the cytokine antibody chips, then incubated with the biotinylated antibody. Cy3 Equivalent Dye-Streptavidin was added, and the fluorescence signals were visualized through a laser scanner equipped with a Cy3 wavelength (InnoScan 300 Microarray Scanner; Innopsys). The mean fluorescent signals of each group containing three repeats were analyzed with specific software Q-Analyzer Tool (code: QAM-CAA-4000) provided by RayBiotech, Inc. The cytokines (FC ≥2 or FC ≤0.5; Table I) were noted by functional category, comprehensively referring to the COSMIC database (http://cancer. sanger.ac.uk/cosmic/), GeneCards database (http://www. genecards.org/), NCBI Gene database (https://www.ncbi.nlm. nih.gov/gene/), and references (25-31).

Statistical analysis. SPSS software version 17.0 (SPSS, Inc.) was used for all analysis. Results are expressed as the means ± SEM. One-way ANOVA was performed to test the null hypothesis of group differences with post hoc tests (Dunnett's test) and unpaired Student's t-test was also performed. P<0.05 was considered to indicate a statistically significant difference. The F-value, which represents the significance of the whole fitting equation and was used to assess the differences between groups, was analyzed using One-way ANOVA.

Results

ORFV strain NA1/11 infects CRC cells and inhibits proliferation. We used the ORFV strain NA1/11, isolated from an outbreak in northeast China, to infect human CRC cells (LoVo, Caco-2, HCT116, RKO, SW480 and SW1116) with multiplicities of infection (MOI) of 0 (mock), 1, 5, 10. After 24 h, cytopathic lesions were observed in some CRC cells, including rounding and swelling (Fig. S1). A recombinant orf virus, NA1/11Δ132-GFP, was used to infect human CRC cells. Then, 24 h post infection (h.p.i.), GFP was visible in the CRC cells (Fig. 1A). In addition, it was determined, via western blotting, that both viral protein ORFV086, which is a proteolytic protein, and GFP reporter protein were expressed at 18 h.p.i in the CRC cells (Fig. 1B).

The crystal violet assay revealed that the total number of cells was decreased when LoVo or CT26 cells were infected by ORFV (Fig. 2A and B). To investigate whether inhibition of proliferation was involved in response to ORFV, CCK-8 assays were performed (Fig. 2C and D). ORFV inhibited the proliferation of LoVo and CT26 in a dose-dependent manner. Notably, the inhibitory effect was not obvious at 24 h.p.i., but increasingly significant at 48 and 72 h.p.i. ORFV also inhibited the proliferation of Caco-2, HCT116, RKO, SW480 and SW1116 cells (Fig. S2).

ORFV strain NA1/11 inhibits the migration of CRC cells. The influence of ORFV on the migration of LoVo and CT26 cells was assessed via a wound healing assay. The cells were cultured at high density in medium containing 10% FBS. After 24 h of serum-starvation, a scratch was made in the confluent cells and the cells incubated for an additional 24 h in medium containing 10% FBS, with or without ORFV treatment. ORFV decreased the migration of the cells into the denuded area, compared to the control (P<0.05; Figs. 3A, B and S3A, B). However, the morphological changes and wound healing assay differences among multiple MOIs of virus infection were small, probably due to insufficient infection time.

Cadherin is associated with tumor progression and metastasis (32). E-cadherin homophilic binding can lead to contact-mediated inhibition of growth, thus the loss of E-cadherin expression is often associated with tumor metastasis (33). On the contrary, N-cadherin promotes the metastatic behavior of tumor cells by directly mediating cell-cell adhesion (34). Thus, it was examined whether E-cadherin and N-cadherin are involved in increased cytotoxicity of ORFV. As anticipated, ORFV treatment caused a significant increase in the expression of E-cadherin. A reduction of N-cadherin was observed in CRC cells incubated with ORFV (Figs. 3C and S3C), indicating that ORFV regulated the expression of cadherins to inhibit the migration of CRC cells.

ORFV strain NA1/11 reduces in vivo tumor growth and metastasis. To investigate the tumoricidal activity of ORFV strain NA1/11 in CRC cells, CT26 cells were injected subcutaneously into BALB/c mice for the development of transplanted tumors. When the tumor size was 25-30 mm³, the mice were treated with ORFV or PBS (Fig. 4A). Consistent with the *in vitro* results, ORFV strain NA1/11 significantly inhibited *in vivo* tumor growth (Fig. 4B) and reduced the tumor size (Fig. 4C). Compared to the PBS-treated group, the average tumor volume decreased significantly in the ORFV-treated group. In addition, CT26 cells were injected into the tail vein of Balb/c mice for the development of a CRC lung metastasis model (Fig. 4D). After three ORFV or PBS treatments, the lungs were harvested (Fig. 4E) and subjected to H&E staining. The average tumor area ratio in lung biopsies of the ORFV-treated group significantly decreased in comparison with those from PBS-treated group (Fig. 4F and G).

ORFV strain NA1/11 alters cytokine secretion. To explore the mechanism of ORFV inhibition of cancer cell growth and metastasis, the ORFV-induced cytokine expression was detected via cytokine antibody chip analysis. After three ORFV or PBS treatments, mice sera were collected from lung metastasis models on the 11th day (Fig. 4D) and subjected
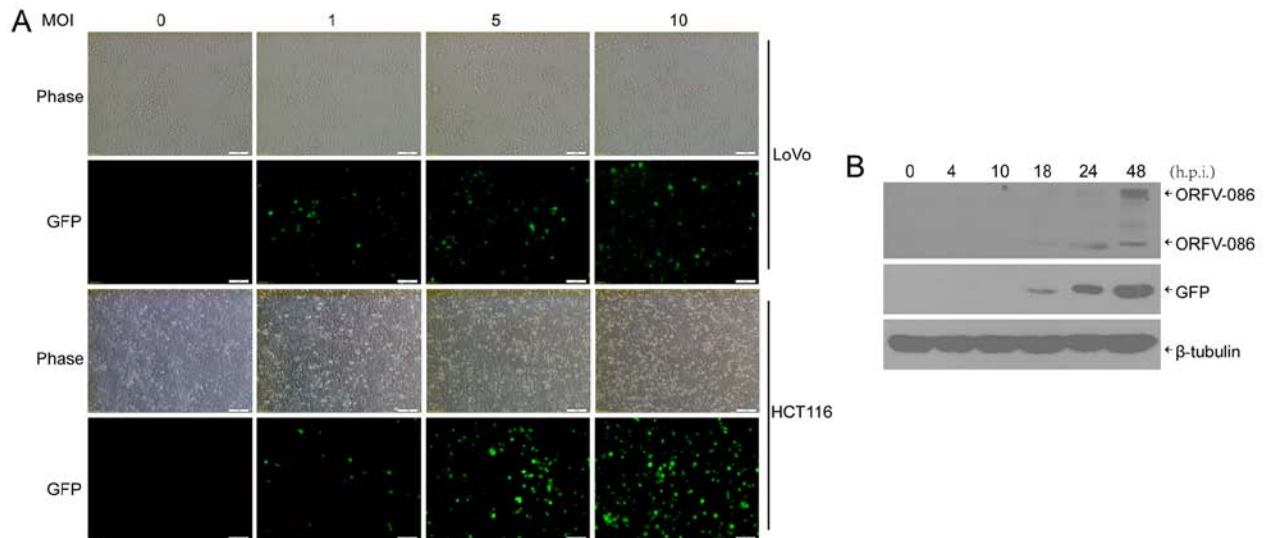
Figure 1. ORFV-infected CRC cells. (A) The CRC cell lines (LoVo and HCT116) were infected with NA1/11Δ132-GFP at an MOI of 5. The images were obtained 24 h post infection. (B) LoVo cells were infected with NA1/11Δ132-GFP (MOI =5) over the indicated time-points, and the whole cell lysates were separated by SDS-PAGE and analyzed by immunoblotting with the indicated antibodies. ORFV, Orf virus; CRC, colorectal cancer; MOI, multiplicity of infection; h.p.i, hours post infection.
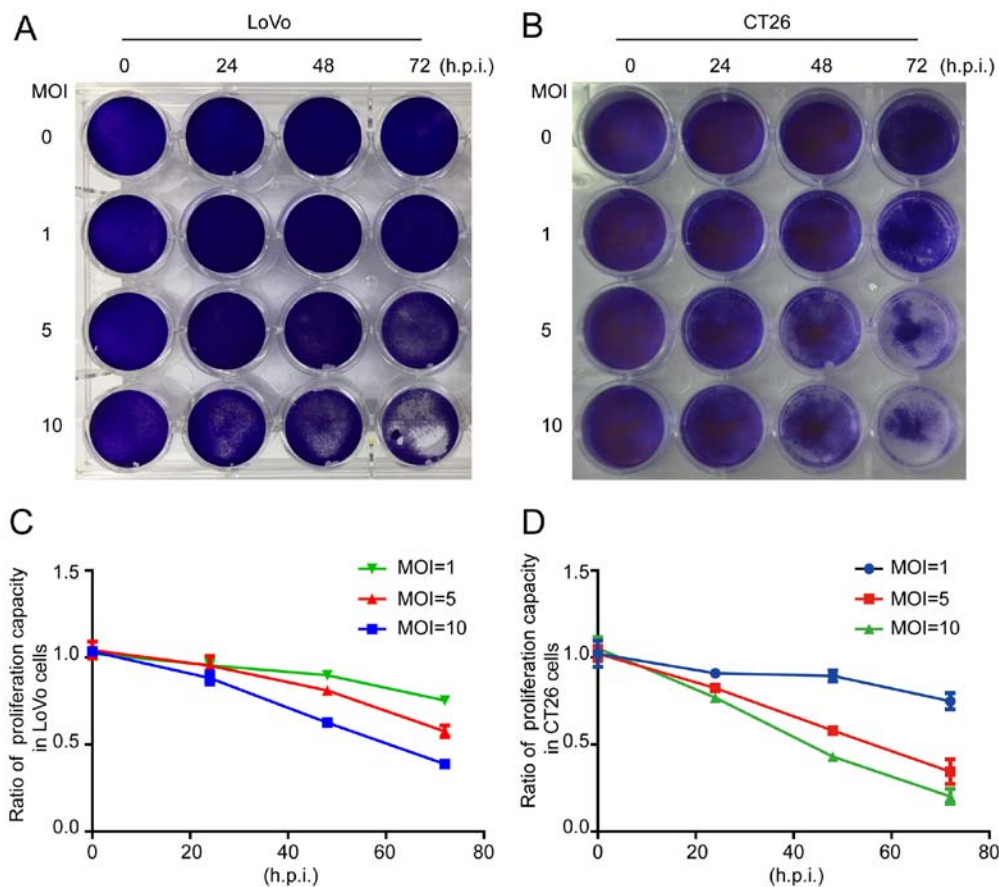

Figure 2. ORFV inhibits *in vitro* proliferation of CRC cells. (A and B) The LoVo and CT26 cells were infected with ORFV at MOI of 0, 1, 5 and 10, and then stained by crystal violet. (C and D) The CCK-8 assay was performed to detect the effect of ORFV on proliferation in LoVo and CT26 cells. ORFV, Orf virus; CRC, colorectal cancer; MOI, multiplicities of infection; CCK-8, Cell Counting Kit-8; h.p.i, hours post infection.

to semi-quantitative cytokine antibody chip assays with 200 cytokines.

The detection images (Fig. 5A) were scanned and converted to a concentration unit. Fold-changes between the ORFV-treated and PBS-treated groups were calculated. A total of 42 cytokines (FC ≥2 or FC ≤0.5; Table I) were sorted into different clusters according to functional annotation, and the forehead clusters of cytokines with the largest numbers were

Table I. Differentially expressed cytokines (fold change ≥2 or ≤0.5) were associated with regulation of apoptosis, angiogenesis, autoimmunity/inflammation, and the cell cycle after the ORFV infection.

Cytokine	F-value	P-value	Fold change	Mean (ORFV-infected, n=3)	Mean (control, n=3)	Functional classification
IL-15	0.000	0.184	2,189.610	827.6	0.4	Apoptosis, angiogenesis, and autoimmunity/inflammation
IL-13	0.000	0.342	1,869.543	402.6	0.2	Autoimmunity/inflammation
RAGE	0.000	0.190	562.576	49.2	0.1	MAPK signaling, ERK1/2 and p53/TP53 signaling and NF-κB
EDAR	0.000	0.282	372.656	3,807.4	10.2	Apoptosis and NF-κB
MIG	0.000	0.114	353.760	359.9	1.0	Transfection factor and TOLLR
TRAIL	0.000	0.250	289.072	321.7	1.1	Apoptosis, angiogenesis, and cell cycle
BLC (CXCL13)	0.000	0.133	219.855	111.9	0.5	Apoptosis and autoimmunity/inflammation
IL-7	0.000	0.306	200.395	185.2	0.9	Apoptosis and autoimmunity/inflammation
CD27	0.000	0.080	185.302	471.6	2.5	Apoptosis, Autoimmunity/inflammation, and cell cycle
Tryptase ε	0.000	0.197	180.294	1,374.2	7.6	Immune response
CCL6	0.000	0.117	156.765	2,374.0	15.1	Chemokine
DLL4	0.002	0.018	64.517	6,938.8	107.6	Angiogenesis, Notch
Fractalkine	0.001	0.370	48.519	15,760.2	324.8	Immune response
TARC	0.001	0.198	36.512	56.8	1.6	Autoimmunity/inflammation
DAN	0.000	0.184	34.164	2,324.7	68.0	Autoimmunity/inflammation and cell cycle
VEGF-D	0.001	0.317	32.318	46.4	1.4	Notch, angiogenesis, and cell cycle
OX40 ligand	0.002	0.205	25.443	245.5	9.6	Apoptosis, autoimmunity/inflammation
Prostasin	0.013	0.258	20.023	2,087.1	104.2	Trypsin-like cleavage specificity
I-TAC	0.063	0.071	11.777	96.6	8.2	Transfection factor, TOLLR, apoptosis, angiogenesis, and autoimmunity/inflammation
Leptin	0.006	0.429	11.208	960.1	85.7	Apoptosis, autoimmunity/inflammation, and angiogenesis
TIM-1	0.071	0.192	9.311	111.9	12.0	Immune response
IL-21	0.299	0.002	9.142	91.7	10.0	Autoimmunity/inflammation
TREM-1	0.272	0.021	9.061	42.5	4.7	Chemokine
H60	0.089	0.044	7.084	95.2	13.4	MHC I
TPO	0.370	0.017	6.500	192.7	29.6	Growth factor
KC	0.551	0.002	5.892	234.5	39.8	Angiogenesis, autoimmunity/inflammation
TACI	0.006	0.150	5.619	78.9	14.0	Apoptosis
ALK-1	0.638	0.005	3.444	67.2	19.5	Protein kinase
BAFF R	0.058	0.004	3.272	100.8	30.8	Immune response
Osteoactivin	0.291	0.035	3.211	1,234.1	384.4	Growth factor
Pentraxin 3	0.012	0.164	3.115	5,956.9	1,912.4	Apoptosis and autoimmunity/inflammation
Granzyme B	0.131	0.096	2.767	406.0	146.7	Apoptosis and autoimmunity/inflammation
Prolactin	0.805	0.069	2.419	2,615.6	1,081.4	Insulin1 and apoptosis
VEGF R1	0.841	0.007	2.236	942.3	421.4	Angiogenesis and protein kinase
Neprilysin	0.698	0.081	2.184	1,059.8	485.2	Apoptosis and angiogenesis
CD30	0.049	0.190	2.152	110.5	51.4	Apoptosis and angiogenesis
Axl	0.874	0.093	0.469	682.5	1,455.8	Protein kinase, apoptosis, and cell cycle
CXCL16	0.252	0.010	0.389	28.8	74.2	Chemokine
ANG-3	0.967	0.031	0.369	120.1	325.4	Tyrosine kinase signaling pathway
MMP10	0.630	0.035	0.369	39.6	107.4	Tumor metastasis
IFN-γ R1	0.225	0.034	0.316	5.3	16.8	The JAK/STAT signaling pathway
VEGF-B	0.063	0.027	0.080	9.1	113.0	Angiogenesis and cell cycle

ORFV, Orf virus; VEGF, vascular endothelial growth factor; DLL4, delta-like canonical Notch ligand 4; BLC, B lymphocyte chemoattractant; IL, interleukin; RAGE, receptor of advanced glycosylation end product; MMP10, matrix metallopeptidase 10.
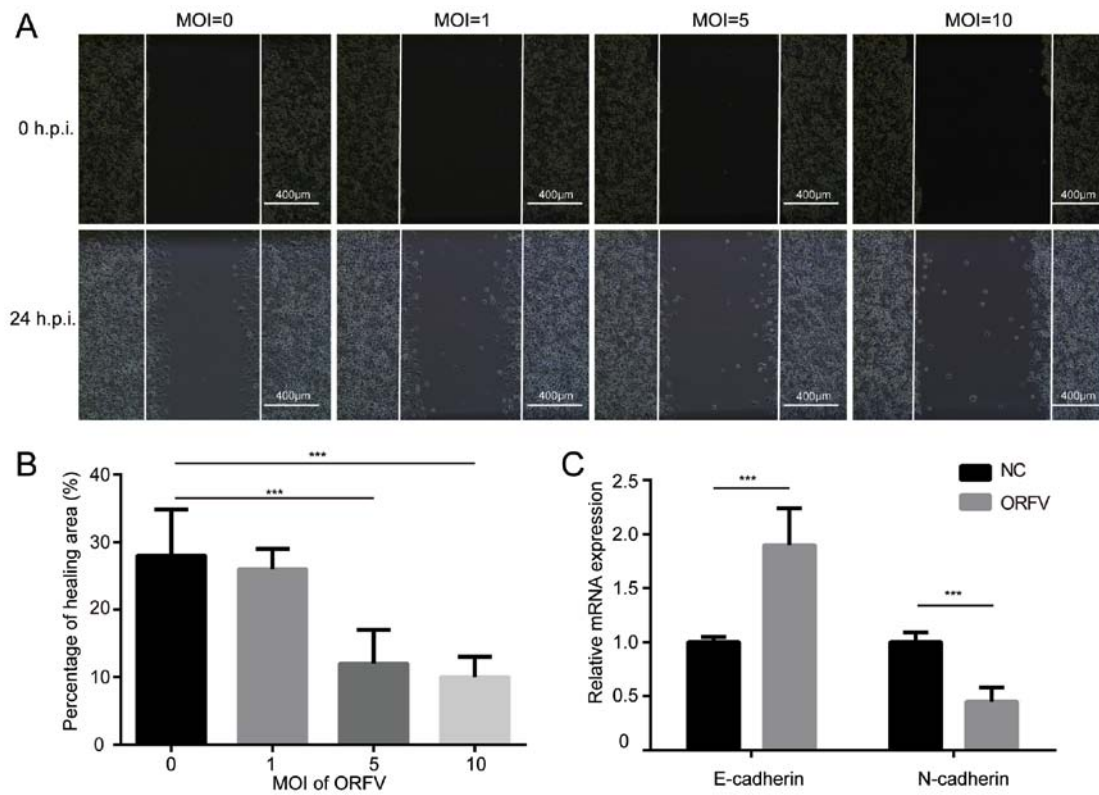
Figure 3. ORFV inhibits the *in vitro* migration of CRC cells. (A) LoVo cells were seeded in 6-well plates at a density of $1x10^6$ cells/well and cultured for 24 h. A wound was scratched in the cell lawn with a 200-μl pipette tip and the cells were exposed to ORFV at designated MOI of 0, 1, 5 and 10. Images of wound healing were captured at 24 h post infection and (B) the percentage of healing areas were calculated. (C) The mRNA expression of E-cadherin and N-cadherin was detected by RT-qPCR in CT26 cells, 24 h post infection. ***$P<0.05$. ORFV, Orf virus; CRC, colorectal cancer; MOI, multiplicities of infection; RT-qPCR, reverse transcription-quantitative PCR; h.p.i, hours post infection.
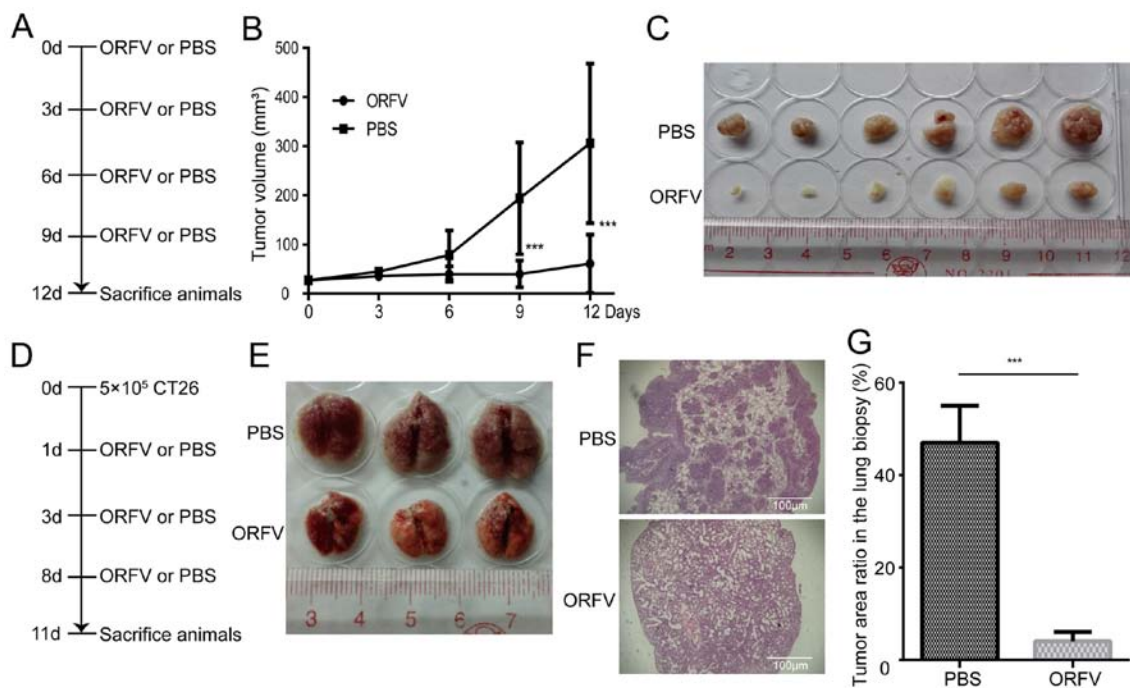
Figure 4. Oncolytic effect of ORFV in a CRC mouse model. (A) A CRC mouse model was established by subcutaneous injection of $5x10^5$ CT26 cells into Balb/c mice. When the tumor size reached 25-30 mm³, 12 mice were divided into two groups and treated with ORFV ($1x10^8$ the median TCID$_{50}$) or PBS by intratu-moral injection. After 12 days, all mice were sacrificed and the tumor tissues harvested. (B) The growth curve of the tumors is presented. (C) Representative images of the excised tumors from the tumor model is presented. (D) Schematic outlining of the treatment schedule for the metastatic lung tumor models. Balb/c mice (n=12) were challenged with $5x10^5$ CT26 cells i.v. and dosed three times with ORFV ($1x10^7$) as indicated. At day 11 after cell injection, lungs were excised. (E) Representative images of the lungs from animals treated with three doses of ORFV or PBS control is presented. (F) Representative images of the lungs by H&E staining. (G) The tumor area ratio in the lung biopsy was calculated in the different groups. ***$P<0.05$. ORFV, Orf virus; CRC, colorectal cancer; TCID$_{50}$, tissue culture infective dose; i.v., intravenously; H&E, hematoxylin and eosin; h.p.i, hours post infection.
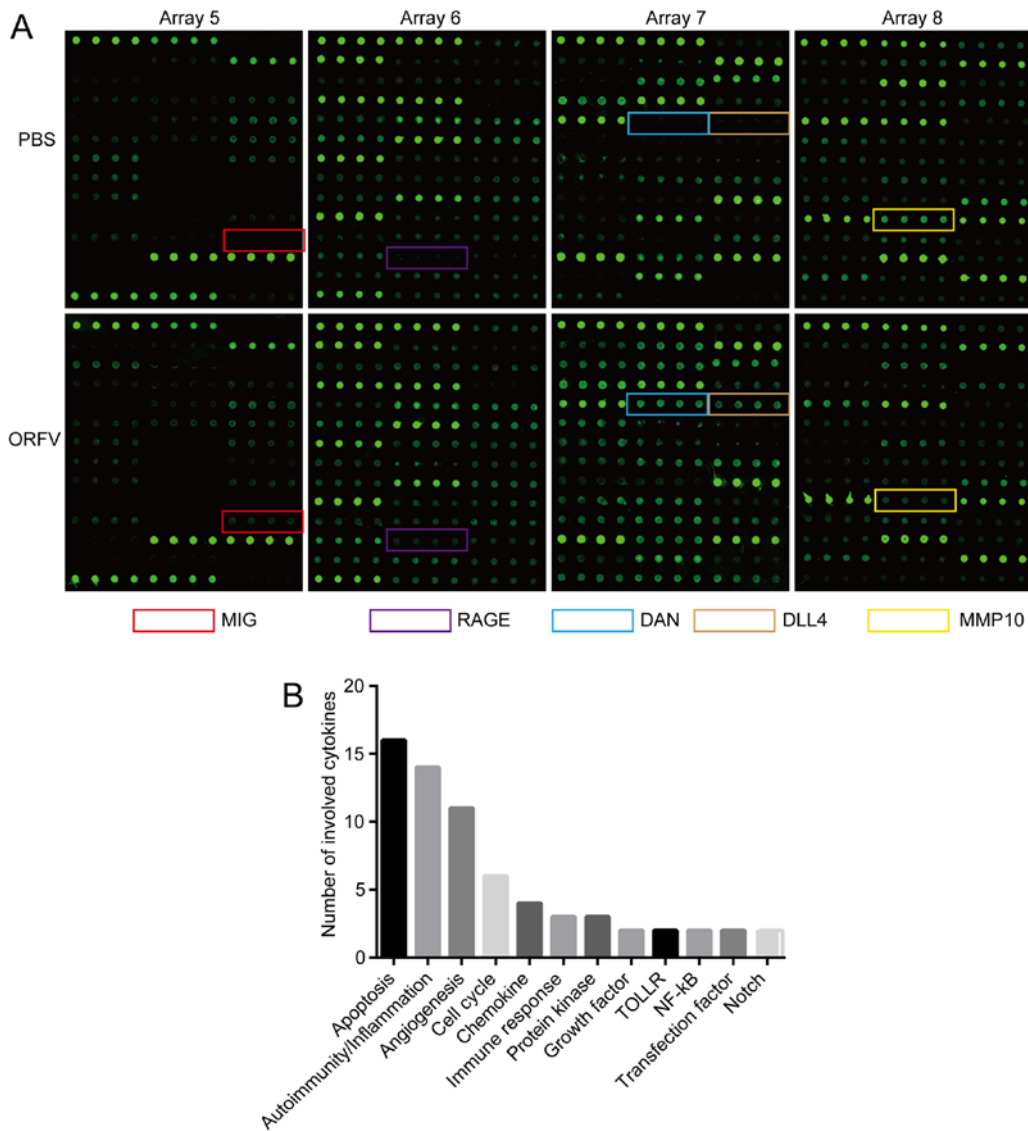
Figure 5. Cytokine microarray identification of serum biomarkers for regulation of oncolysis. Mice sera of the ORFV-treated and PBS-treated subjects were collected and measured, according to the manufacturer's instructions, with a semi-quantitative mouse cytokine antibody array. (A) The upper panels represent the samples treated with PBS, while the lower panels represent the samples treated with ORFV. Arrays 5-8 represent different panels of microarrays which were embedded with antibodies against distinct cytokines. (B) The numbers of cytokines classified by distinct function. ORFV, Orf virus; RAGE, receptor of advanced glycosylation product; MMP10, matrix metallopeptidase 10; DLL4, delta-like canonical Notch ligand 4.

autoimmunity/inflammation, apoptosis, angiogenesis, and the cell cycle. The fold-change sorting of these cytokines and brief functional annotations are presented in Fig. 5B. Notably, for the individual differences in the mice, the results of cytokine antibody chips array revealed that a variety of cytokines with large fold changes were not statistically significant (Table I). The results of cytokine antibody chip assay indicated that NA1/11 may play roles in those cytokines and direct the preliminary direction for our future research. These cytokines must be further confirmed in additional studies.

ORFV strain NA1/11 induces CRC cell apoptosis. Among differentially expressed cytokines screened by cytokine antibody chip analysis, apoptosis-related cytokines were in the majority. There were 15 upregulated cytokines and 1 down-regulated cytokine related to apoptosis in the ORFV-treated group. Thus, apoptosis was examined by three distinct approaches. Using flow cytometry, apoptotic cells were

revealed to be significantly increased in the ORFV-stimulated group compared to the PBS-treated group (Fig. 6A). Western blot analysis revealed that apoptosis-regulated proteins Smac, cleaved caspase-3, cleaved caspase-9 and cleaved PARP were significantly enhanced in LoVo cells incubated with ORFV virus from 0 to 48 h.p.i. (Fig. 6B).

To examine whether the antitumor activity of ORFV was due to the potentiation of apoptosis *in vivo*, the tumor tissues from the mouse model were analyzed by IHC assay. Consistent with the *in vitro* results, the expression of cleaved caspase-3 in tumor tissues from the ORFV-treated group was significantly increased compared to that of tumor tissues from the PBS-treated groups (Fig. 6C and D).

Discussion

There are some unique biological characteristics which make ORFV an attractive oncolytic virus vector. First, the ORFV
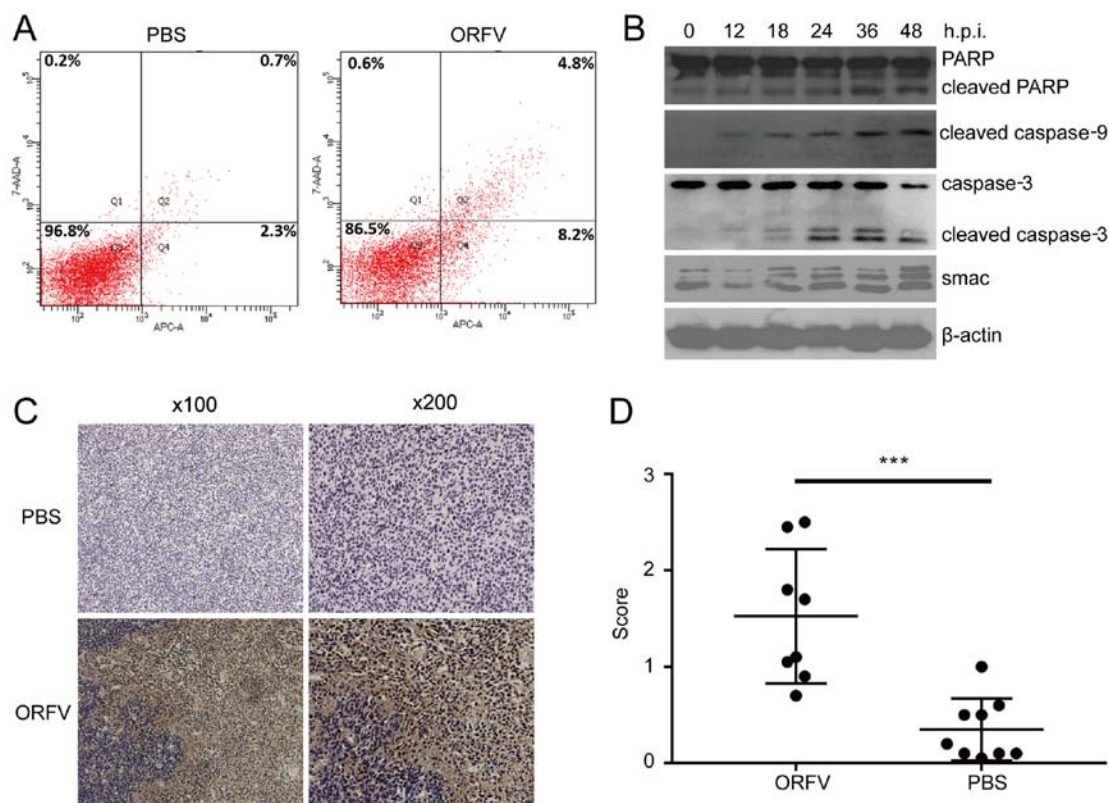
Figure 6. ORFV induces apoptosis in CRC cells. (A) LoVo cells were seeded at a density of 1×10^6 cells/well in 6-well plates and exposed to ORFV (MOI =5) or PBS for 24 h. Flow cytometry detected apoptosis in CT26 cells by Annexin V-APC/7-ADD staining. (B) LoVo cells were exposed to ORFV (MOI =5) for 0, 12, 18, 24, 36 and 48 h. Total protein of cells was used to detect the expression of the cleaved PARP, cleaved caspase-9, cleaved caspase-3 and Smac by western blotting. (C) Apoptosis of tumor cells was assessed and quantified by immunohistochemistry (cleaved caspase-3). (D) Immunistochemical score. ***P<0.05. ORFV, Orf virus; CRC, colorectal cancer; MOI, multiplicity of infection.

genes are replicated and transcribed in the cytoplasm rather than integrated into the host genome, and thus ORFV is considered relatively safe to develop as an oncolytic virus. Second, the host range of ORFV infection is constricted, its damage is limited mainly to the skin that can recover quickly, and the virus has low toxicity and shows little evidence of systemic transmission. Third, ORFV infection can rapidly mediate humoral and adaptive immune responses, but little neutralizing serum antibody is produced after stimulation by ORFV. Furthermore, attenuated virus strains can be constructed by knockout of the virulence genes. As a viral vaccine vector, the gene compatibility is large, and it can replicate and express exogenous genes. Finally, ORFV infection can cause the release of immunoregulatory molecules, including IFN, IL-2, and TNF. Therefore, ORFV has the potential to be an ideal oncolytic virus vector (9,10,17,19,35,36).

Although ORFV strain NZ2 has been reported to be able to induce anticancer effects in murine cancer models (11), it is necessary to verify the antitumor effect of the ORFV strain NA1/11 for its high variability in the terminal regions of the genome among different strains (37). In the present study, it was first confirmed that ORFV strain NA1/11 could infect and cause typical cytopathic lesions in CRC cell lines. Then, CCK-8 assay indicated that ORFV strain NA1/11 could suppress the proliferation of CRC cells. Furthermore, it was revealed that ORFV strain NA1/11 significantly inhibited the migration of CRC cells. ORFV strain NA1/11 inhibited tumor proliferation and metastasis *in vivo*. A cytokine antibody chip assay was performed to explore the potential mechanism of ORFV, which revealed that apoptosis may play an important role in ORFV-induced cytotoxicity.

Cytokine antibody chip assay revealed the general profile of cytokine regulation. According to functional classification, four groups containing the most numerous cytokines were apoptosis, autoimmunity/inflammation, angiogenesis, and the cell cycle. Some of the cytokines, including IL-15, IL-21, CD27, VEGF-B, delta-like canonical Notch ligand 4 (DLL4), are pleiotropic cytokines that likely play important roles in apoptosis and autoimmunity/inflammation. It is possible that cytokines, such as CCL6, TREM-1, CXCL16, could affect chemotactic activity, inhibition of tumor metastasis or regulation of the NF-κB pathway. More detailed studies are required to depict an integrated regulation network of the ORFV-mediated oncolysis.

Interleukins (ILs) were first discovered to be expressed by leukocytes, which extensively influence the functions of the immune system, such as promoting the development and differentiation of T and B lymphocytes and hematopoietic cells (26). In the present study, IL-15 was the cytokine most markedly altered in the microarray assay, with a fold-change of more than 2000. This cytokine and IL-2 share numerous common functional characteristics, including regulating the activation and proliferation of T cells and NK cells (27,31). IL-15 can also induce the activation of JAK kinases. IL-21 is another interleukin whose expression levels were upregulated in this assay, with a fold-change of 9.142, and plays a

role in both the innate and adaptive immune responses. It can induce the differentiation, proliferation, and activity of various immune cells, including NK cells, macrophages, cytotoxic T cells and B cells, and functions in synergy with IL-15 in some of these regulatory roles (31). IL-21 can stimulate IFN production in T cells and NK cells, and inhibits activation and maturation of DC within T-cell mediated immune responses (28). Analogously, IL-7 may facilitate the functions of the immune system through a similar mechanism (29). These results indicated that interleukins may play a crucial role in the oncolytic effect of ORFV, possibly through regulating the proliferation and activation of T cells, NK cells and other immune cells. CD27, a member of the TNF-receptor superfamily, plays a crucial role in regulating B-cell activation and immunoglobulin synthesis via binding to ligand CD70, and can exert apoptosis-promoting effects through association with the proapoptotic CD27-binding protein (SIVA) (25, 30).

Angiogenesis plays an important role in tumor tissue development and thus has become a key target in various tumor molecular therapy strategies (38,39). The most downregulated cytokine in the microarray assay was VEGF-B, a member of the vascular endothelial growth factor (VEGF) family, which can regulate the formation of blood vessels (angiogenesis) and is involved in the growth of endothelial cells (40). DLL4 is related to the Notch signaling pathway and can negatively regulate the proliferation, migration, and angiogenic sprouting of endothelial cells (41).

Chemokines are a family of small cytokines able to induce directed chemotaxis in adjacent responsive cells, and are classified into four main subfamilies: CXC, CC, CX3C and XC (42). In the present study, the microarray assay results indicated three chemokines, CCL6, TREM-1 and CXCL16, that may take part in ORFV-mediated oncolysis in cancer cells (43-45). For instance, TREM-1 can strengthen neutrophil and monocyte-mediated inflammatory responses, which are triggered by promoting the release of pro-inflammatory chemokines and other cytokines (44). The receptor of advanced glycosylation product (RAGE), a multi-ligand cell surface receptor, was markedly upregulated when cancer cells were treated with ORFV. It can also interact with various molecules involved in homeostasis, development, and inflammation. The MAPK signaling, ERK1/2 signaling, p53/TP53 signaling and NF-κB signaling pathways are important pathways in which RAGE functions (46,47). The cytokine matrix metallopeptidase 10 (MMP10), involved in tissue remodeling and in certain disease processes, is the only cytokine identified to be related to tumor metastasis (48).

Apoptosis is an important cellular process induced or inhibited by viral infection. Apoptosis plays an important role in the antitumor effect (49), and previous studies suggested that apoptosis contributes to the oncolytic effect induced by oncolytic viruses (1,50,51). In the present study, there were 15 upregulated cytokines and 1 downregulated cytokine related to apoptosis in the ORFV strain NA1/11-treated group, consistent with literature studies (30,52-55).

In conclusion, the present results indicated that ORFV strain NA1/11 could inhibit CRC growth and metastasis by inducing apoptosis of CRC cells. In addition, ORFV NA1/11s could upregulate serum levels of IL-7, IL-13, IL-15, CD27, CD30, pentraxin 3, and B lymphocyte chemoattractant (BLC or CXCL13) and downregulate Axl, CXCL16, ANG-3, MMP10, IFN-γ R1 and VEGF-B, leading to enhanced oncolytic activity.

Acknowledgements

Not applicable.

Availability of data and materials

The datasets used during the present study are available from the corresponding author upon reasonable request.

Authors' contributions

WH, DC and SL conceived and designed the study. DC, RW, ML, WL, BX, HD, KW, DG and FL performed the experiments. DC, RW, ML, and SL analyzed the data. DC, RW, WH and SL wrote the manuscript. All authors have read and approved the final manuscript.

Ethics approval and consent to participate

All animal procedures were reviewed and approved by the Institutional Animal Care and Use Committee at Foshan University (Foshan, China) (approval no. 20170311).

Patient consent for publication

Not applicable.

Competing interests

The authors declare that they have no competing interests.

References

1. Lawler SE, Speranza MC, Cho CF and Chiocca EA: Oncolytic viruses in cancer treatment: A review. JAMA Oncol 3: 841-849, 2017.
2. Kaufman HL, Kohlhapp FJ and Zloza A: Oncolytic viruses: A new class of immunotherapy drugs. Nat Rev Drug Discov 14: 642-662, 2015.
3. Mondal M, Guo J, He P and Zhou D: Recent advances of oncolytic virus in cancer therapy. Hum Vaccin Immunother 16: 2389-2402, 2020.
4. Raja J, Ludwig JM, Gettinger SN, Schalper KA and Kim HS: Oncolytic virus immunotherapy: Future prospects for oncology. J Immunother Cancer 6: 140, 2018.

5. Liu Z, Ravindranathan R, Kalinski P, Guo ZS and Bartlett DL: Rational combination of oncolytic vaccinia virus and PD-L1 blockade works synergistically to enhance therapeutic efficacy. Nat Commun 8: 14754, 2017.

6. Andtbacka RH, Kaufman HL, Collichio F, Amatruda T, Senzer N, Chesney J, Delman KA, Spitler LE, Puzanov I, Agarwala SS, et al: Talimogene laherparepvec improves durable response rate in patients with advanced melanoma. J Clin Oncol 33: 2780-2788, 2015.

7. Hosamani M, Scagliarini A, Bhanuprakash V, McInnes CJ and Singh RK: Orf: An update on current research and future perspectives. Expert Rev Anti Infect Ther 7: 879-893, 2009.

8. Wang R, Wang Y, Liu F and Luo S: Orf virus: A promising new therapeutic agent. Rev Med Virol 29: e2013, 2019.

9. Fiebig HH, Siegling A, Volk HD, Friebe A, Knolle P, Limmer A and Weber O: Inactivated orf virus (Parapoxvirus ovis) induces antitumoral activity in transplantable tumor models. Anticancer Res 31: 4185-4190, 2011.

10. van Rooij EM, Rijsewijk FA, Moonen-Leusen HW, Bianchi AT and Rziha HJ: Comparison of different prime-boost regimes with DNA and recombinant Orf virus based vaccines expressing glycoprotein D of pseudorabies virus in pigs. Vaccine 28: 1808-1813, 2010.

11. Rintoul JL, Lemay CG, Tai LH, Stanford MM, Falls TJ, de Souza CT, Bridle BW, Daneshmand M, Ohashi PS, Wan Y, et al: ORFV: A novel oncolytic and immune stimulating parapoxvirus therapeutic. Mol Ther 20: 1148-1157, 2012.

12. Friebe A, Friederichs S, Scholz K, Janssen U, Scholz C, Schlapp T, Mercer A, Siegling A, Volk HD and Weber O: Characterization of immunostimulatory components of orf virus (parapoxvirus ovis). J Gen Virol 92: 1571-1584, 2011.

13. Tai LH, de Souza CT, Bélanger S, Ly L, Alkayyal AA, Zhang J, Rintoul JL, Ananth AA, Lam T, Breitbach CJ, et al: Preventing postoperative metastatic disease by inhibiting surgery-induced dysfunction in natural killer cells. Cancer Res 73: 97-107, 2013.

14. Breitbach CJ, Paterson JM, Lemay CG, Falls TJ, McGuire A, Parato KA, Stojdl DF, Daneshmand M, Speth K, Kirn D, et al: Targeted inflammation during oncolytic virus therapy severely compromises tumor blood flow. Mol Ther 15: 1686-1693, 2007.

15. Cai J, Lin Y, Zhang H, Liang J, Tan Y, Cavenee WK and Yan G: Selective replication of oncolytic virus M1 results in a bystander killing effect that is potentiated by Smac mimetics. Proc Natl Acad Sci USA 114: 6812-6817, 2017.

16. Warner SG, Haddad D, Au J, Carson JS, O'Leary MP, Lewis C, Monette S and Fong Y: Oncolytic herpes simplex virus kills stem-like tumor-initiating colon cancer cells. Mol Ther Oncolytics 3: 16013, 2016.

17. Weber O, Mercer AA, Friebe A, Knolle P and Volk HD: Therapeutic immunomodulation using a virus - the potential of inactivated orf virus. Eur J Clin Microbiol Infect Dis 32: 451-460, 2013.

18. Haig DM and McInnes CJ: Immunity and counter-immunity during infection with the parapoxvirus orf virus. Virus Res 88: 3-16, 2002.

19. Chen D, Long M, Xiao B, Xiong Y, Chen H, Chen Y, Kuang Z, Li M, Wu Y, Rock DL, et al: Transcriptomic profiles of human foreskin fibroblast cells in response to orf virus. Oncotarget 8: 58668-58685, 2017.

20. Wang Y, Tong S, Li W, Gao F, Ning Z and Luo S: In vitro cultivation of primary ovine fetal turbinate cells and its application in researches of ovine orf virus. Zhongguo Shouyi Kexue 43: 470-475, 2013 (In Chinese).

21. Li W, Ning Z, Hao W, Song D, Gao F, Zhao K, Liao X, Li M, Rock DL and Luo S: Isolation and phylogenetic analysis of orf virus from the sheep herd outbreak in northeast China. BMC Vet Res 8: 229, 2012.

22. LaBarre DD and Lowy RJ: Improvements in methods for calculating virus titer estimates from $TCID_{50}$ and plaque assays. J Virol Methods 96: 107-126, 2001.

23. Ning Z, Peng Y, Hao W, Duan C, Rock DL and Luo S: Generation of recombinant Orf virus using an enhanced green fluorescent protein reporter gene as a selectable marker. BMC Vet Res 7: 80, 2011.

24. Livak KJ and Schmittgen TD: Analysis of relative gene expression data using real-time quantitative PCR and the 2(-Delta Delta C(T)) method. Methods 25: 402-408, 2001.

25. Akiba H, Nakano H, Nishinaka S, Shindo M, Kobata T, Atsuta M, Morimoto C, Ware CF, Malinin NL, Wallach D, et al: CD27, a member of the tumor necrosis factor receptor superfamily, activates NF-kappaB and stress-activated protein kinase/c-Jun N-terminal kinase via TRAF2, TRAF5, and NF-kappaB-inducing kinase. J Biol Chem 273: 13353-13358, 1998.

26. Brocker C, Thompson D, Matsumoto A, Nebert DW and Vasiliou V: Evolutionary divergence and functions of the human interleukin (IL) gene family. Hum Genomics 5: 30-55, 2010.

27. Gaffen SL and Liu KD: Overview of interleukin-2 function, production and clinical applications. Cytokine 28: 109-123, 2004.

28. Kuchen S, Robbins R, Sims GP, Sheng C, Phillips TM, Lipsky PE and Ettinger R: Essential role of IL-21 in B cell activation, expansion, and plasma cell generation during CD4+ T cell-B cell collaboration. J Immunol 179: 5886-5896, 2007.

29. Or R, Abdul-Hai A and Ben-Yehuda A: Reviewing the potential utility of interleukin-7 as a promoter of thymopoiesis and immune recovery. Cytokines Cell Mol Ther 4: 287-294, 1998.

30. Prasad KV, Ao Z, Yoon Y, Wu MX, Rizk M, Jacquot S and Schlossman SF: CD27, a member of the tumor necrosis factor receptor family, induces apoptosis and binds to Siva, a proapoptotic protein. Proc Natl Acad Sci USA 94: 6346-6351, 1997.

31. Steel JC, Waldmann TA and Morris JC: Interleukin-15 biology and its therapeutic implications in cancer. Trends Pharmacol Sci 33: 35-41, 2012.

32. Wang B, Tan Z and Guan F: Tumor-derived exosomes mediate the instability of cadherins and promote tumor progression. Int J Mol Sci 20: 3652, 2019.

33. Petrova YI, Schecterson L and Gumbiner BM: Roles for E-cadherin cell surface regulation in cancer. Mol Biol Cell 27: 3233-3244, 2016.

34. Mrozik KM, Blaschuk OW, Cheong CM, Zannettino AC and Vandyke K: N-cadherin in cancer metastasis, its emerging role in haematological malignancies and potential as a therapeutic target in cancer. BMC Cancer 18: 939, 2018.

35. Voigt H, Merant C, Wienhold D, Braun A, Hutet E, Le Potier MF, Saalmüller A, Pfaff E and Büttner M: Efficient priming against classical swine fever with a safe glycoprotein E2 expressing Orf virus recombinant (ORFV VrV-E2). Vaccine 25: 5915-5926, 2007.

36. Fischer T, Planz O, Stitz L and Rziha HJ: Novel recombinant parapoxvirus vectors induce protective humoral and cellular immunity against lethal herpesvirus challenge infection in mice. J Virol 77: 9312-9323, 2003.

37. Li W, Hao W, Peng Y, Duan C, Tong C, Song D, Gao F, Li M, Rock DL and Luo S: Comparative genomic sequence analysis of Chinese orf virus strain NA1/11 with other parapoxviruses. Arch Virol 160: 253-266, 2015.

38. Aruga A: Current status and future perspective of cancer immunotherapy - clinical application and development. Nihon Geka Gakkai Zasshi 114: 327-331, 2013 (In Japanese).

39. Lapeyre-Prost A, Terme M, Pernot S, Pointet AL, Voron T, Tartour E and Taieb J: Immunomodulatory activity of VEGF in cancer. Int Rev Cell Mol Biol 330: 295-342, 2017.

40. Poesen K, Lambrechts D, Van Damme P, Dhondt J, Bender F, Frank N, Bogaert E, Claes B, Heylen L, Verheyen A, et al: Novel role for vascular endothelial growth factor (VEGF) receptor-1 and its ligand VEGF-B in motor neuron degeneration. J Neurosci 28: 10451-10459, 2008.

41. Shutter JR, Scully S, Fan W, Richards WG, Kitajewski J, Deblandre GA, Kintner CR and Stark KL: Dll4, a novel Notch ligand expressed in arterial endothelium. Genes Dev 14: 1313-1318, 2000.

42. Fernandez EJ and Lolis E: Structure, function, and inhibition of chemokines. Annu Rev Pharmacol Toxicol 42: 469-499, 2002.

43. Abel S, Hundhausen C, Mentlein R, Schulte A, Berkhout TA, Broadway N, Hartmann D, Sedlacek R, Dietrich S, Muetze B, et al: The transmembrane CXC-chemokine ligand 16 is induced by IFN-gamma and TNF-alpha and shed by the activity of the disintegrin-like metalloproteinase ADAM10. J Immunol 172: 6362-6372, 2004.

44. Bouchon A, Dietrich J and Colonna M: Cutting edge: Inflammatory responses can be triggered by TREM-1, a novel receptor expressed on neutrophils and monocytes. J Immunol 164: 4991-4995, 2000.

45. Ma B, Zhu Z, Homer RJ, Gerard C, Strieter R and Elias JA: The C10/CCL6 chemokine and CCR1 play critical roles in the pathogenesis of IL-13-induced inflammation and remodeling. J Immunol 172: 1872-1881, 2004.

46. Hermani A, De Servi B, Medunjanin S, Tessier PA and Mayer D: S100A8 and S100A9 activate MAP kinase and NF-kappaB signaling pathways and trigger translocation of RAGE in human prostate cancer cells. Exp Cell Res 312: 184-197, 2006.

47. Dahlmann M, Okhrimenko A, Marcinkowski P, Osterland M, Herrmann P, Smith J, Heizmann CW, Schlag PM and Stein U: RAGE mediates S100A4-induced cell motility via MAPK/ERK and hypoxia signaling and is a prognostic biomarker for human colorectal cancer metastasis. Oncotarget 5: 3220-3233, 2014.

48. Upadhyay P, Gardi N, Desai S, Chandrani P, Joshi A, Dharavath B, Arora P, Bal M, Nair S and Dutt A: Genomic characterization of tobacco/nut chewing HPV-negative early stage tongue tumors identify MMP10 asa candidate to predict metastases. Oral Oncol 73: 56-64, 2017.
49. Croce CM and Reed JC: Finally, an apoptosis-targeting therapeutic for cancer. Cancer Res 76: 5914-5920, 2016.
50. Loya SM and Zhang X: Enhancing the bystander killing effect of an oncolytic HSV by arming it with a secretable apoptosis activator. Gene Ther 22: 237-246, 2015.
51. Wei X, Liu L, Wang G, Li W, Xu K, Qi H, Liu H, Shen J, Li Z and Shao J: Potent antitumor activity of the Ad5/11 chimeric oncolytic adenovirus combined with interleukin-24 for acute myeloid leukemia via induction of apoptosis. Oncol Rep 33: 111-118, 2015.
52. Raeber ME, Zurbuchen Y, Impellizzieri D and Boyman O: The role of cytokines in T-cell memory in health and disease. Immunol Rev 283: 176-193, 2018.
53. Vial J, Royet A, Cassier P, Tortereau A, Dinvaut S, Maillet D, Gratadou-Hupon L, Creveaux M, Sadier A, Tondeur G, *et al*: The ectodysplasin receptor EDAR acts as a tumor suppressor in melanoma by conditionally inducing cell death. Cell Death Differ 26: 443-454, 2019.
54. Huang ZM, Du SH, Huang LG, Li JH, Xiao L and Tong P: Leptin promotes apoptosis and inhibits autophagy of chondrocytes through upregulating lysyl oxidase-like 3 during osteoarthritis pathogenesis. Osteoarthritis Cartilage 24: 1246-1253, 2016.
55. Yuan X, Gajan A, Chu Q, Xiong H, Wu K and Wu GS: Developing TRAIL/TRAIL death receptor-based cancer therapies. Cancer Metastasis Rev 37: 733-748, 2018.